energies

MDPI

Article

Effect of the Solid Particle Diameter on Frictional Loss and Heat Exchange in a Turbulent Slurry Flow: Experiments and Predictions in a Vertical Pipe

Artur S. Bartosik

Department of Production Engineering, Kielce University of Technology, Al. Tysiaclecia P.P. 7, 25-314 Kielce, Poland; artur.bartosik@tu.kielce.pl

Abstract: The study deals with experiments and predictions on turbulent flow and heat exchange in a fully developed slurry flow in a vertical upward pipe. Four slurries were considered: two with glass spheres particles with diameters of 0.125 mm and 0.240 mm, respectively, and two with sand spheres particles with diameters of 0.470 mm and 0.780 mm, respectively. The volume concentration of the particles was changed in the range of 10% to 40%. This study has indirectly demonstrated the existence of turbulence suppression to a degree dependent on the diameter of the solid particles. A mathematical model for heat transfer between slurry and pipe was developed using the two-equation turbulence model and a specially designed wall function, including particle diameter and solid concentration. The model assumed a constant wall temperature and heat flux. The study's objective was to determine the influence of the diameter of the solid particles on the heat exchange. The Nusselt number was found to change sinusoidal, reaching a maximum for a slurry with d = 0.125 mm, and a minimum for d = 0.470 mm. The higher the solid concentration, the lower the Nusselt number. The novelty and value of this study lies in the deeper characterisation and understanding of the influence of the diameter of solid particles on heat exchange.

Keywords: vertical slurry flow; damping of turbulence; influence of solid particle on heat exchange

Citation: Bartosik, A.S. Effect of the Solid Particle Diameter on Frictional Loss and Heat Exchange in a Turbulent Slurry Flow: Experiments and Predictions in a Vertical Pipe. *Energies* **2023**, *16*, 6451. https://doi.org/10.3390/en16186451

Academic Editor: Dmitry Eskin

Received: 29 July 2023
Revised: 3 September 2023
Accepted: 4 September 2023
Published: 6 September 2023

1. Introduction

Slurry flow has interested scientists and engineers for centuries [1]. Slurries occur widely in chemical and mining industries. The influence of temperature on slurry friction is of relevance for the mining industry. In some cases, mineral extraction is carried out at a temperature of 200 °C and the tailings from this process are pumped at a temperature of 70 °C [2]. Many engineering companies design, construct, and operate long-distance slurry pipelines [3,4].

Slurry flow depends on Reynolds number, solid concentration, bulk and settling velocities, pipe diameter, physical properties of the solid and liquid phases, particle size distribution, and flow geometry [5,6]. As a result of this complexity, engineers are constantly looking for new methods to better understand solid–liquid and solid–solid interactions. They are interested in a simple useful mathematical model for parametric studies [7–9].

Solid particles in the liquid affect the shear stresses on the wall and the erosion and abrasion of the pump and pipeline components [10–12]. Solid particles also affect the carrier liquid's turbulence and the heat exchange intensity [13,14]. It is well known that slurries with fine solid particles are responsible for increased viscosity and yield shear stress. In such a case, rheological measurements are necessary to determine the viscosity, yield stress, and proper rheological model. However, when considering a slurry with medium or coarse solid particles, it is accepted that the mathematical model includes the viscosity of the carrier phase, as the rheological properties cannot be measured because the sedimentation process is too intensive [5,15]. This phenomenon is pronounced if the density of the solid particle increases. If the density of medium or coarse solid particles is higher than that of carrier liquid, the particles settle under gravity, but they can be fully suspended for sufficiently high velocity.

The importance of the diameter of the solid particles in the carrier liquid remains a challenge for many scientists [16,17]. Experiments on solid–liquid flow are complex, time consuming, and rarely available in the literature. Such experiments require careful preparation of solid particles, including screening or sieving, determining the median particle diameter, and slurry concentration. Running the flow requires degassing the slurry, determining the settling velocity to avoid flow blockages, keeping a constant temperature, determining the mass of the solid particles delivered, and finally, proper measurement instruments and control and monitoring systems. Measurement instruments can be intrusive or non-intrusive [18,19]. Intrusive methods have limitations because measurements at high concentrations of the solid phase result in the risk of damage or contamination of the probe. Moreover, such measures are almost impossible near a pipe wall. Non-intrusive methods, like optics, ultrasounds, or magnetic resonance do not affect the flow structure but they have limitations too. When optical methods are considered, the particles induce attenuation of the beams. However, if the refractive index matches the suspended particles and the carrier fluid, it is possible to perform measurements of particle velocities but for limited solid concentrations. For these reasons, most measurements refer to gas–liquid flows. The newest techniques, like ultrasounds or magnetic resonances, also have limitations. Although these methods propose a relatively good spatial resolution, this is still insufficient to measure the fluctuating parts of the solid and liquid phases [20–23], which is essential for developing more reliable turbulence models. Based on the above, one can say that there is still an alternative to using standard turbulence models together with a specially designed wall damping function. The wall damping function can be developed based on comparing predictions and measurements of global parameters, such as frictional loss and velocity and temperature distributions. This approach was used in the current studies.

The main objective of the study is to determine the influence of the diameter of the solid particles on the heat exchange between a pipe and a turbulent slurry flow in the upward vertical pipeline. Four slurries were studied—two slurries with glass spheres and two slurries with sand particles. The median particle diameters of the respective slurries were 0.125 mm, 0.240 mm, 0.470 mm, and 0.780 mm. Solid volume concentrations changed in the range of 10% to 40%.

The novelty and value of this study lies in the deeper characterisation and understanding of the influence of the diameter of solid particles on heat exchange. In addition, the novelty of this article lies in proposing a simple physical and mathematical model, which includes the median particle diameter and solids concentration. This model is suitable for parametric studies, which allow us to simulate the effect of solid particle diameter, solid concentration, heat flux, wall temperature, and physical and thermal properties of solid and liquid phases on heat exchange efficiency between pipe and turbulent slurry flow. The study presents the results and analysis of measurements and numerical predictions, which include $dp/dx = f(U_b)$, $T = f(y)$, $Nu = f(Re)$, and $Nu = f(d)$.

1.1. Literature Review: Isothermal Flow

Solid particles in a carrier liquid result in a slip velocity between the solid and liquid phases. Yianneskis and Whitelaw [24] pioneered LDA measurements for fully developed turbulent pipe flow for a slurry with solid particles of a median diameter of 0.27 mm. The authors noted that there are no significant differences in the velocity of the liquid and solid phases. Furthermore, the importance of slip velocity decreased with increasing solid concentration. However, slip velocity is generally essential in dilute slurries, that is, in slurries with low solid concentration or in slurries with sufficiently high particle diameter and density [25,26].

Some researchers conducted studies on the behaviour of solid particles near a pipe wall [27–30]. They commonly concluded that the ejection-sweep cycle near a pipe wall is strongly affected by solid particles. Furthermore, the authors emphasised that solid particles can enhance or suppress turbulence. Researchers such as Gore and Crowe [31], Jianren et al. [32], Eaton et al. [33], Fessler and Eaton [34], and Li et al. [35] emphasised the influence of solid particles on the modulation of turbulence. In general, we have obtained sufficient research results that confirm that the behaviour of solid particles in a liquid can led to the increase or suppression of turbulence. However, no function has been determined allowing us to clearly state whether we deal with the suppression or enhancement of turbulence.

Li et al. [35] analysed the effect of adding large solid particles to a flat plate boundary layer that was spatially developed on the transport characteristics of slurries. The authors compared the slurry transport characteristics at different flow rates and different solid concentrations of glass spheres with a median particle size of 0.125 mm before and after adding the same volume fraction of glass spheres of 0.44 mm. They analysed the particle velocity distribution, the turbulent kinetic energy of the small particles, and the wall shear forces. The authors found that adding 0.44 mm particles decreased the turbulent kinetic energy of the small particles and significantly reduced the total resistance of the pipe by 10% at the bulk velocity of 4 m/s and the solid volume concentration by 20%. Matousek et al. [36] formulated similar conclusions with a slurry containing solid particles with sizes of 0.22 mm and 1.56 mm.

Javed et al. [37,38] performed experiments on the frictional behaviour of the slurry in a horizontal flow. The authors considered two grades of sand and glass spheres with median particle diameters of 0.103, 0.447, and 0.5 mm, respectively, and straw with a nominal particle length of 19.2 mm. The friction loss of the slurry measured in the vertical pipe of bulk velocities in the range of 0.5–4.2 m/s and mass concentrations in the range of 5–25% showed a reduction of 19% in drag at the solid concentration of 25% and at the bulk velocity of 3.5 m/s [37,38].

Experiments on medium- and coarse-solid particles suspended in a carrier liquid demonstrate the significant influence of particle diameter on the solid concentration distribution across a pipe. Nasr-El-Din et al. [39] and Sumner et al. [40] proved that in a vertical flow, the distribution of solids depends on the diameter of the particle and decreases when approaching the pipe wall. When the average diameter of the solid particles increases, the concentration profile becomes more inhomogeneous, showing a clear tendency to reach a minimum value near the pipe wall. In this case, the frictional loss was lower than expected. The authors also demonstrated that solid phase concentration profiles are uniform if fine solid particles are used [39,40].

The results mentioned above coincide with those obtained by other researchers, such as Eaton and Fessler [41] and Eskin and Miller [42]. For example, Eskin and Miller [42] proposed an original approach to describe the dynamics of a solid particle at the microscopic level for the case where a slurry flows through a gap. Their model showed that the dynamics of the solid particles in the carrier liquid is due to the fluctuation of the solid particles in the region of high shear rate. They found that solid particles migrate from the area of high to the area of low shear rate, resulting in the flow being characterised by a nonuniform distribution of the solid particles in the cross-section. The authors also found that the reduced concentration of the solid phase at the crack wall, due to particle migration, reduces friction loss comparing to a flow in which the distribution of the solid particles was homogeneous. In conclusion, the flow of the slurry through the gap was characterised by a lower pressure drop than expected [42].

Silva et al. [43] and Cotas et al. [44] used commercial CFD software to simulate eucalyptus and pine pulps fully developed turbulent flow; as such, slurries exhibit drag reduction. They applied a pseudo-homogeneous approach. The authors adopted the turbulence model of Chang et al. [45], in which they used the turbulence-damping function proposed by Bartosik [46]. They validated the mathematical model by comparing the measured and predicted friction pressure loss with decent accuracy.

Based on the gathered knowledge, concerning an isothermal slurry flow with medium or coarse solid particles, one can say that the median particle diameter has a significant influence on turbulence. However, this phenomenon is complex because many parameters, such as particle diameter, solid concentration, flow conditions, flow geometry, and properties of the solid and liquid phases, affect turbulence. This complexity leads to the need for research on medium and coarse slurry flows and mathematical models that are simple and relevant for engineering applications. The majority of mathematical models, which use a single- or two-phase approach, apply a standard two-equation turbulence model together with a commercial code [47,48]. Too little attention is paid to the phenomenon of slurry flow and the importance of physical features, which usually results in solving 3D governing equations, even though it is not justified. It is useless to apply a mathematical model to predict heat exchange in a slurry flow if the model was not positively validated for the isothermal flow first.

1.2. Literature Review: Non-Isothermal Flow

Most available data on heat exchange in slurry flows refer to low and moderate solid concentrations, and laminar flow. In contrast, data for high solid concentrations, which are of particular interest in the long-distance transportation of minerals, are difficult to access [49,50]. Reliable prediction first requires reliable measurement. Therefore, experiments on medium and coarse slurry flows are still expected, and the ability to simulate a slurry flow to predict frictional losses, velocity, and temperature distribution remains one of the main challenges of computational fluid dynamics.

The influence of the diameter of solid particles on heat exchange in a turbulent slurry flow has been experimentally investigated by several researchers [51–55]. For example, Mandal et al. [51] theoretically analysed the effect of particle size on fluid flow and heat transfer using the commercial code Fluent. The authors considered a fly ash slurry flow with median particle diameters of 0.012, 0.020, 0.028, and 0.034 mm in a horizontal pipe. They performed computations at a constant bulk density equal to 4 m/s and a volume concentration of 40%. The authors found that granular pressure and heat transfer increase with particle size. Other experiments on the heat transfer coefficient in a slurry transported in a horizontal pipe were performed by Rozenblit et al. [55]. The authors focused on the flow of the acetyl–water mixture on a moving bed with solid volume concentrations ranging from 5% to 15%. The authors used an electro-resistance sensor and infrared imaging to measure the temperature profile on the heated wall. The authors observed that the local heat transfer coefficient changed from its lowest value at the bottom of the pipe to the highest value at the upper heterogeneous layer [55].

Based on the literature, it can be noted that most of the research on heat transfer in solid–liquid flow refers to ice slurry and slurries with fine solid particles and colloidal suspensions, called nanofluids. Nanofluids have been known for several decades and were designed to improve heat exchange in some engines and heat exchangers [56–59]. Wang et al. [60] carried out experiments on the thermal conductivity of Al_2O_3 and CuO nanoparticles mixed with water, vacuum pump liquid, engine oil, and ethylene glycol [60]. The authors used Al_2O_3 with a median particle diameter of 28 nm and CuO with a median particle diameter of 23 nm. All particles were loosely agglomerated in the chosen liquid. The authors proved that the thermal conductivity of the mixture depends on the properties of the liquid and solid phases and increases with increasing solid volume concentration [60].

Recently, Cieslinski [47] reviewed the achievements in numerical modelling of forced convection in nanofluids in round and smooth tubes. The author noted that most mathematical models assume constant heat flux acting on a chosen pipe length and constant wall temperature. In the single-phase approach, the mixture of nanoparticles and carrier liquid is treated as homogeneous; therefore, the thermophysical properties are those of a nanofluid. In the two-phase approach, the thermophysical properties of the nanoparticles and carrier liquid are applied independently. In the review of mathematical models, the author selected only those that have been validated. The mathematical models mainly described suspension of nanoparticles of Al_2O_3, CuO, Cu, SiO_2, TiO_2, ZrO_2 and water as a carrier liquid. The author recognised 30 mathematical models for single-phase flows and 23 for two-phase flows. Cieslinski [47] stated that some researchers, such as, for example, Lotfi et al. [61] and Mokmeli and Saffar-Avval [62] observed that the precision of a single-phase approach is similar to that of a two-phase approach. The problem of closing the governing equations was solved using the standard k-ε turbulence model. The author stated that some available simulations indicated an improvement in heat transfer caused by carefully selected solid particles, while some did not [47].

Summarising the literature review on isothermal and non-isothermal slurry flow, one can say that the research is focused on fine slurry or laminar flows [48], while data for slurries with medium and coarse solid particles are rarely available. Furthermore, the mathematical models used for the prediction of slurry flow mainly rely on standard turbulence models and do not take into account the influence of the particle diameter and solid concentration on turbulence. Due to the limited access to experimental data on the behaviour of solid particles at the pipe wall in a broad range of solid particles and solid concentrations, we still face limitations in predicting velocity and temperature distributions. In the absence of reliable data for turbulence, especially near a pipe wall over a wide range of solid concentrations and particle diameters, it is difficult to suggest a new turbulence model. However, it is possible to modify existing turbulence models to predict the pressure drop, velocity, and temperature distributions in a slurry flow.

2. Method of Analysis

For the purpose of this study, the measurements of the isothermal slurry flow with glass spheres, carried out by Shook and Bartosik [63], and sand particles, carried out by Sumner [40], were chosen. The experiments were carried out in a closed vertical loop made of clear PVC in the upward direction. The vertical pipe was straight and smooth, and its inner diameter was 26 mm. The experimental test rig of these experiments is presented in Figure 1. All solid particles used in experiments were closely sized; that is, the particles had a narrow diameter distribution. The particles suspended in water were round, smooth, and rigid. Four slurries were studied—two of them contained medium, while two other, coarse solid particles. The following solid particles were used in this study:

a. Medium solid particles:
   - glass spheres with median diameter d = 0.125 mm and particle density ρ_P = 2440 kg/m^3;
   - glass spheres with median diameter d = 0.240 mm and particle density ρ_P = 2440 kg/m^3.

b. Coarse solid particles:
   - sand with median diameter d = 0.470 mm and particle density rP = 2650 kg/m^3;
   - sand with median diameter d = 0.780 mm and particle density rP = 2650 kg/m^3.

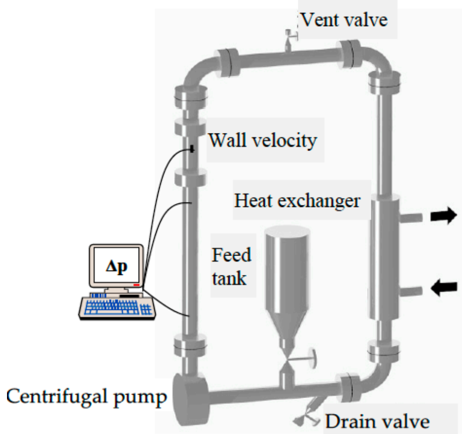

Figure 1. Experimental test rig; upward vertical slurry flow [63]. Source: own elaboration.

2.1. Physical Model

To develop a mathematical model for heat exchange in a slurry containing the aforementioned solid particles, a physical model must be formulated first. To build a simple mathematical model, it is better to consider a vertical pipe flow, because such a flow is axially symmetric, which simplifies the model. Therefore, in this study, a straight vertical pipeline was used, and the slurry flow was in the upward direction. The cylindrical coordinate system has been used in the mathematical model (x, r, θ), where '0x' is the symmetry axis of the pipe and represents the main flow direction, while the radial coordinate '0r' represents the distance from the symmetry axis. In this study, the coordinate '0θ', which represents the angle around the symmetry axis, will not be considered, which is the result of assumptions.

The physical model of slurry flow in the upward vertical pipeline was developed based on the following assumptions:

- The slurry flow is carried out in a straight vertical pipeline in the upward direction; the diameter of the inner pipe is equal to 0.026 m.
- The flow is steady, turbulent, axially symmetric ($V = 0$ and $\partial V/\partial r = 0$) and without circumferential eddies ($W = 0$ and $\partial W/\partial \varphi = 0$).
- The flow of the slurry is fully developed hydrodynamically, which means that the time-averaged velocity component U does not change in the flow direction ($\partial U/\partial x = 0$).
- The wall temperature is constant and equal to $T_w = 293.15$ K.
- The heat flux is constant, homogeneous, and equal to $q = 1500$ W/m; the heat flux acts from the pipe wall towards the symmetry axis.
- The slurry flow is fully thermally developed, which means that the temperature changes linearly in the flow direction 'ox', $\partial T/\partial x = \text{const} \neq 0$.
- Heat production in a slurry is negligible.
- Heat conduction through the pipe wall and radiation were neglected.
- The viscosity of the carrier liquid (water) was determined for the temperature of the pipe wall.
- The thermal properties of the solid particles are constant.
- The distribution of solid concentration in the cross-section of the pipe is constant.
- The single-phase approach is applied.
- The density of the slurry, the conduction coefficient, and the specific heat are constant and were determined from the temperature of the wall using Equation (1). Therefore, it was arbitrarily assumed that $(T_w – T_b) < 5$ K.

$$\Phi_m = C\Phi_S + (1 - C)\Phi_L \tag{1}$$

where T_b is the bulk temperature (averaged over the pipe cross-section); Φ is a general dependent variable that represents the density, heat conduction, or specific heat of the slurry; C is the volume concentration of solids, while the subscripts m, S, L refer to slurry (mixture), solid, and liquid, respectively.

The physical properties of the solid and liquid phases are presented in Table 1, while the physical properties of the slurries are shown in Table 2.

Table 1. The physical properties of solid and liquid phases.

Name	d, mm	ρ, kg/m^3	μ, Pa s	c_p, J/(kg K)	λ, W/(m K)
Carrier liquid	0.000	998.32	0.0010046	4180.90	0.598
Glass spheres particles	0.125 0.240	2440.00		729.00	1.047
Sand particles	0.470 0.780	2650.00		712.00	1.088

where d is the median diameter of solid particles; ρ is the density of carrier liquid or slurry; μ is the dynamic viscosity of the carrier liquid; c_p is specific heat at constant pressure; λ is the thermal conductivity of the carrier liquid or solid particles.

Table 2. The physical properties of slurries.

Name	C, %	ρ_m, kg/m^3	$(c_p)_m$, J/(kg K)	λ_m, W/(m K)
Slurry with glass spheres particles	10	1142.49	3835.71	0.643
	30	1430.82	3145.33	0.733
	40	1574.99	2800.14	0.778
Slurry with sand particles	10	1163.49	3834.01	0.647
	30	1493.82	3140.23	0.745
	40	1658.99	2793.34	0.794

where ρ_m is the slurry density; $(c_p)_m$ is the specific heat of the slurry at constant pressure, and λ_m is the thermal conductivity of the slurry.

2.2. Mathematical Model

Taking into account the rules of time-averaging and neglecting terms with fluctuating components of density and viscosity, one can formulate the general governing equations of mass, momentum, and internal energy for steady vertical flow in the upward direction.

$$\frac{\partial}{\partial x_i}\left(\overline{\rho}\overline{U}_i\right) = 0 \tag{2}$$

$$\frac{\partial}{\partial x_j}\left(\overline{\rho}\overline{U_i U_j}\right) = -\frac{\partial \overline{p}}{\partial x_i} + \frac{\partial}{\partial x_j}\left(\mu \frac{\partial \overline{U}_i}{\partial x_j} - \overline{\rho}\,\overline{u_i' u_j'}\right) - \overline{\rho} g_i \tag{3}$$

$$\frac{\partial}{\partial x_j}\left(\overline{\rho}\overline{U}_j\overline{T}\right) = \frac{\partial}{\partial x_j}\left(\frac{\mu}{Pr}\frac{\partial \overline{T}}{\partial x_j}\right) - \frac{\partial}{\partial x_j}\left(\overline{\rho}\,\overline{u_j' t'}\right) \tag{4}$$

where U is the time-averaged velocity; p is the static pressure; μ and ρ are the dynamic viscosity and density of the transported medium, respectively; g is specific gravity; $\overline{\rho}\overline{u_i' u_j'}$ is the turbulence stress tensor; T is time averaged temperature; $\overline{\rho}\overline{u_j' t'}$ is fluctuating component of velocity and temperature, and Pr is the Prandtl number defined as:

$$\mathrm{Pr} = \frac{\mu\, c_p}{\lambda} \tag{5}$$

Solving the set of equations requires that the number of equations is equal to the number of dependent variables. This approach is called the closure problem. The momentum and energy Equations (3) and (4) possess the components $-\overline{\rho}\overline{u_i' u_j'}$ and $-\overline{\rho}\overline{u_j' t'}$, which are unknown and require closure. Both components can be modelled using a direct (DNS) or indirect approach. The direct method gives a high level of accuracy but is more complex and requires long computation times. Additionally, this method considers random velocity and random temperature, which is not pragmatic for most engineering applications. The indirect method gives fair accuracy in numerical prediction but is less complex and needs a much shorter computation time. In addition, the indirect method considers the time-averaged velocity and temperature, which is more relevant in engineering applications. Therefore, an indirect method was used in this study. Taking into account the Boussinesque concept, we can write [64]:

$$-\overline{\rho}\,\overline{u_i' u_j'} = \mu_t\left(\frac{\partial \overline{U}_i}{\partial x_j} + \frac{\partial \overline{U}_j}{\partial x_i}\right) - \frac{2}{3}\,\overline{\rho}\,k\,\delta_{i,j} \tag{6}$$

where k is the kinetic energy of the turbulence; $\delta_{i,j}$ is the Kronecker quantity; μ_t is the turbulent viscosity.

The fluctuating components in Equations (3) and (4) can be described using Equation (6) as:

$$-\overline{\rho}\,\overline{u'v'} = \mu_t\,\frac{\partial \overline{U}}{\partial r} \tag{7}$$

$$-\overline{\rho}\,\overline{u_j' t'} = \frac{\mu_t}{Pr_t}\frac{\partial \overline{T}}{\partial x_i} \tag{8}$$

where u′ and v′ are fluctuating parts of the velocities in the ox and or direction, respectively; U is the component of the time-averaged velocity in the ox direction, Pr_t is the turbulent Prandtl number for the boundary layer equal to $Pr_t = 0.9$ [65].

Taking into account the assumptions stated in the physical model, the final form of Equations (2)–(4), together with Equations (7) and (8), can be expressed as follows.

$$\frac{\partial}{\partial x}(\overline{\rho}_m \overline{U}) = 0 \tag{9}$$

$$\frac{1}{r}\frac{\partial}{\partial r}\left[r\,(\mu+\mu_t)\frac{\partial \overline{U}}{\partial r}\right] = \frac{\partial \overline{p}}{\partial x} + \rho_m g \tag{10}$$

$$\overline{\rho}_m \overline{U}\frac{\partial \overline{T}}{\partial x} = \frac{1}{r}\frac{\partial}{\partial r}\left[r\left(\frac{\mu}{Pr}+\frac{\mu_t}{Pr_t}\right)\frac{\partial \overline{T}}{\partial r}\right] \tag{11}$$

The turbulent viscosity μ_t in Equation (10) was calculated using the turbulence model of Launder and Sharma [66]. The Launder–Sharma model was successfully validated for many turbulent flows, including homogeneous slurries. Researchers emphasised that it is one of the first and most widely used models. It has been shown to agree well with measurements and DNS data for a wide range of turbulent flows and performs better than many other k-ε models [67–71]. Launder and Sharma expressed the turbulent viscosity as follows [66]:

$$\mu_t = f_\mu \frac{\overline{\rho}}{\varepsilon} k^2 \tag{12}$$

$$f_\mu = 0.09\, exp\left[\frac{-3.4}{\left(1+\frac{Re_t}{50}\right)^2}\right] \tag{13}$$

where f_m is called the damping function of the turbulence or the wall damping function. The turbulent Reynolds number (Re_t) was developed from the dimensionless analysis [66], as follows:

$$Re_t = \frac{\rho\, k^2}{\mu\, \varepsilon} \tag{14}$$

where ε is the dissipation of the kinetic energy of turbulence.

The turbulence damping Function (13) was determined for homogeneous turbulence [68]. It will be demonstrated that using Function (13) for the chosen slurries gives a higher friction than the measurements. Therefore, a specially designed turbulence-damping function was used for medium and coarse slurries. The turbulence-damping function applied in the mathematical model is the following [46]:

$$f_\mu = 0.09\left\{\frac{-3.4\,\left[1 + A_P^3\, d^2 (8 - 88\, A_P\, d)\, C^{0.5}\right]}{\left(1+\frac{Re_t}{50}\right)^2}\right\} \tag{15}$$

where A_P is an empirical constant ($A_P = 100$).

Function (15) was developed empirically by matching the predictions of friction loss and velocity distribution with the measurements. This function was validated for isothermal flows for medium and coarse slurries in the range of median particle diameters of 0.1 to 0.8 mm and solid concentrations of 10% to 40%, obtaining good accuracy of predictions of friction losses and velocity profiles [46,69,70,72,73].

Analysis of Equation (15) indicates that if d→0 or C→0 the turbulence-damping function approaches the standard function expressed by Equation (13). Equation (15) indicates that the median particle diameter of the solid particle plays a primary role, while the solid concentration plays a secondary role.

Considering the assumptions made in the physical model, the final forms of the equations of the kinetic energy of turbulence and its dissipation rate in the cylindrical coordinate system are as follows.

$$\frac{1}{r}\frac{\partial}{\partial r}\left[r\left(\mu+\frac{\mu_t}{\sigma_k}\right)\frac{\partial k}{\partial r}\right]+\mu_t\left(\frac{\partial\overline{U}}{\partial r}\right)^2=\rho\varepsilon+2\mu\left(\frac{\partial k^{1/2}}{\partial r}\right)^2 \tag{16}$$

$$\frac{1}{r}\frac{\partial}{\partial r}\left[r\left(\mu+\frac{\mu_t}{\sigma_\varepsilon}\right)\frac{\partial \varepsilon}{\partial r}\right]+C_1\frac{\varepsilon}{k}\mu_t\left(\frac{\partial\overline{U}}{\partial r}\right)^2=C_2\left[1-0.3\,exp\left(-Re_t^2\right)\right]\frac{\rho\varepsilon^2}{k}-2\frac{\mu}{\rho}\mu_t\left(\frac{\partial^2\overline{U}}{\partial r^2}\right)^2 \tag{17}$$

where C_1, and C_2 are constants; σ_k and σ_ε are diffusion coefficients in the equations of k and ε, respectively.

According to the assumptions, the convective term in the energy Equation (11) requires a unique approach. To develop the convective term, consider the energy balance between the pipe, with inner diameter D and unit length L = 1 m, and the slurry in the pipe. The heat flux, which is transferred from the pipe to the slurry, can be expressed as

$$\dot{Q}=\alpha\,A_*\,\Delta\overline{T}_r \tag{18}$$

where α is the coefficient of convective heat transfer; $\Delta\overline{T}_r=T_w-T_b$ is temperature difference on radius r, and

$$A_*=\pi DL \tag{19}$$

The changes in the inner energy of the slurry over the pipe distance L are as follows.

$$\dot{Q}=\dot{m}\,c_P\,\Delta\overline{T}_x=\overline{\rho}_b\,\overline{U}_b\,A\,c_p\,\Delta\overline{T}_x \tag{20}$$

where $\dot{m}$ is flux of slurry mass; $\Delta\overline{T}_x$ is the slurry temperature difference over the pipe distance Δx = L; $\overline{\rho}_b$ and $\overline{U}_b$ are bulk density and velocity, respectively; the $A = \pi D^2/4$ is the cross section of the pipe.

Comparing the right-hand side of Equation (18) with the right-hand side of Equation (20) and including (19), one can write:

$$\alpha\,\pi\,D\,L\,\Delta\overline{T}_r=\overline{\rho}_b\,\overline{U}_b\,\pi\,\frac{D^2}{4}\,c_p\,\Delta\overline{T}_x \tag{21}$$

Dividing each side of Equation (21) by the unit length L = Δx, we get

$$\dot{q}=\overline{\rho}_b\,\overline{U}_b\,\pi\,\frac{D^2}{4}\,c_p\,\frac{\Delta\overline{T}_x}{\Delta x} \tag{22}$$

where q is the unit heat flux.

Finally, ∂T/∂x, which exists in the energy Equation (11), can be expressed as follows:

$$\frac{\partial\overline{T}}{\partial x}=\frac{\dot{q}}{\overline{\rho}_b\,\overline{U}_b\,\pi\,R^2c_p}=const \tag{23}$$

where R is the radius of the pipe.

The gradient ∂T/∂x, described in Equation (23), was applied in Equation (11). The thermal properties of the carrier liquid and solid phases used in the computations are known and are listed in Tables 1 and 2.

The final form of the mathematical model of heat exchange in the turbulent flow of medium and coarse slurries in an upward vertical pipeline constitutes four partial differential equations, namely, (10), (11), (16), and (17). The model has complementary Equations (12), (14), (15), and (23). The constants in the k-ε turbulence model are the same as in the Launder and Sharma model and are the following: C_1 = 1.44; C_2 = 1.92; σ_k = 1.0; σ_ε = 1.3 [66]. The mathematical model contains five dependent variables: U(r), p(x), T(r), k(r), ε(r), and has four partial differential equations only. The closure problem was solved by assuming that the pressure gradient ∂p/∂x is given. Therefore, the mathematical model was solved for the pre-set value of ∂p/∂x. By changing ∂p/∂x, one can change the bulk velocity. This approach allows one to make the mathematical model one-dimensional and reduce the computation time.

2.3. Numerical Procedure

The following boundary conditions were applied in the numerical computations:

$$\text{pipe wall, r = R:} \quad \text{q = 1500 W/m; } T_w = 293.15\text{ K; U = 0; k = 0; } \varepsilon = 0; \tag{24}$$

$$\text{symmetry axis, r = 0:} \quad \partial T/\partial r = 0;\ \partial U/\partial r = 0,\ \partial k/\partial r = 0 \text{ and } \partial\varepsilon/\partial r = 0. \tag{25}$$

Equation (24) indicates that the wall temperature is constant and there is no slip on the pipe wall (U = k = ε = 0), while Equation (25) indicates that axially symmetric conditions were applied to the dependent variables. The set of partial differential Equations (10), (11), (16) and (17) was solved by the TDMA method with the iteration procedure and the finite-volume method [74] and using its own computer code. The finite volume was established for a pipe with a length of L = 1 m, and by rotating its radius around the symmetry axis at an angle of φ = 1 radian. The numerical computations require initial dependent variables, which were calculated as follows.

- $T(r) = T_w$;
- $U(r) = U_{max}[(R - r)/R]^{1/7}$;
- k was established on the basis of the assigned intensity of turbulence, that is, $k(r) = 1/2\, U^2(r)$;
- ε was established based on the equation: $\varepsilon(r) = 0.09^{3/4}\, k^{3/2}(r)/L$, where L was determined from the Nikuradse formula [75].

The iterative convergence criterium was defined by Equation (26).

$$\sum_j \left| \frac{\varnothing_j^n - \varnothing_j^{n-1}}{\varnothing_j^n} \right| \leq 0.001 \tag{26}$$

where $\varnothing_j^n$ is a general dependent variable ∅ = U, T, k, ε; the jth is the nodal point after the nth iteration cycle, and the $\varnothing_j^{n-1}$ is the (n − 1)th iteration cycle.

The number of grid points strongly affects the accuracy of the predictions [74,76]. Therefore, the following meshes containing 60, 70, 80, and 90 nodal points distributed on a pipe radius were applied. Additionally, the expansion coefficient has been used to achieve a nonuniform distribution of nodal points on a pipe radius, so most nodal points were located close to a pipe wall. It was found that for the expansion coefficient equal to 1.1, the iterative convergence process for 80 and 90 nodal points was similar. For this reason, the mesh with 80 nodal points was used.

The results of numerical computations allowed us to obtain the flow field of the fully developed hydrodynamically and thermally turbulent flow of medium and coarse slurries, which includes the distribution of T(r), U(r), k(r), ε(r). Additionally, the following quantities can be calculated: Nu, Pr, Re, U_b, and T_b.

2.4. Validation for Isothermal Slurry Flow

The mathematical model has been validated for isothermal slurry flows in the range of median particle diameters from d = 0.1 mm to d = 0.8 mm, and solid concentrations of C = 10% to C = 40%, and in a comprehensive range of Reynolds numbers and pipe diameters, giving reasonably good predictions of dp/dx = f(U_b) and velocity profiles [46,69,70,72,73]. To convince the reader that the chosen slurries with medium and coarse solid particles demonstrate the suppression of turbulence and that the mathematical model predicts those flows well, the results of the selected measurements and predictions will be presented.

Figures 2 and 3 show the results of the measured and predicted frictional pressure loss for four slurries, containing particles with diameters of 0.125 mm, 0.240 mm, 0.470 mm, and 0.780 mm, respectively, and for volume concentration of solids equal to 40%. The results of predictions using the modified damping Function (15) are marked as solid red lines, while predictions with the standard damping Function (13) are marked as dashed red lines.

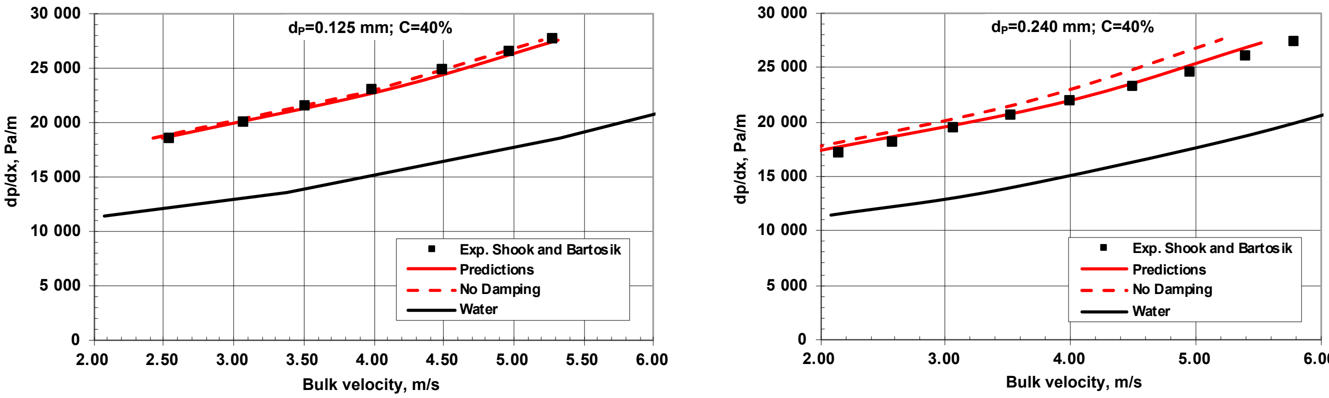

(**a**) (**b**)

Figure 2. Predictions with and without damping of turbulence and measurements [63] for glass spheres slurries: (**a**) d = 0.125 mm, C = 40%, D = 0.026 mm; (**b**) d = 0.240 mm, C = 40%, D = 0.026 mm.

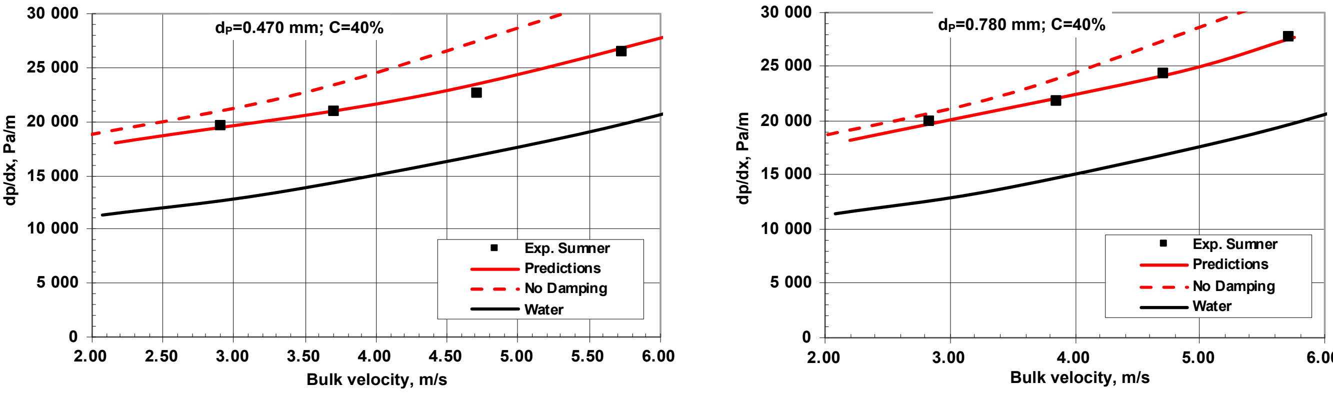

(**a**) (**b**)

Figure 3. Predictions with and without damping of turbulence and measurements [40] for sand slurries: (**a**) d = 0.470 mm, C = 40%, D = 0.026 mm; (**b**) d = 0.780 mm, C = 40%, D = 0.026 mm.

The analysis of Figures 2 and 3 shows discrepancies between the measurements and the numerical predictions if the mathematical model contains a standard wall damping function, described by Equation (13). The disparity increases with increasing particle diameter, and the highest discrepancy appears for the slurry with a solid particle diameter equal to 0.470 mm, as seen in Figure 3a. The predictions with the wall damping Function (15) match well with the measurements for all applied particles, as seen in Figures 2 and 3.

The analysis of Figures 2 and 3 indicates that dp/dx for glass sphere slurry at C = 40% should be approximately 1.57 times higher than water because this slurry's density is equal to 1574 kg/m^3. However, it is approximately 1.52 for d = 0.125 mm and 1.45 for d = 0.240 mm. If the data for the sand slurry with C = 40% (ρ_m = 1658 kg/m^3) are analysed, we expect that dp/dx should be approximately 1.66 higher compared to water, while it is only 1.49 for d = 0.470 mm and 1.51 for d = 0.780 mm. In conclusion, the experimental data presented in Figures 2 and 3 explicitly show that the friction loss of the four slurries depends on the diameter of the particle and is lower than we expected. Therefore, one can conclude that such slurries demonstrate turbulence suppression. The lowest friction loss was obtained for the slurry with d = 0.470 mm.

2.5. Validation for Non-Isothermal Slurry Flow

Due to the lack of experimental data on heat exchange in slurries used in these studies, the mathematical model was validated only for carrier liquid flow. Numerical computations were performed for turbulent carrier liquid flow in a vertical pipe with inner diameter D = 0.026 m, wall temperature T_w = 293.15 K, and unit heat flux q = 1500 W/m. The results of the predicted Nusselt number were compared with the Dittus–Boelter empirical Equation (27) [77] and are presented in Figure 4. The Dittus–Boelter equation is valid for fully developed flows for Re > 10,000 and $0.7 \leq Pr \leq 160$ [77] and is expressed as follows:

$$Nu = 0.02296\, Re^{0.8}\, Pr^{1/3} \tag{27}$$

where Reynolds and Prandtl's numbers are as follows:

$$Re = \frac{\rho\, U_b\, 2\, R}{\mu_L} \tag{28}$$

$$Pr = \frac{\mu_L\, c_p}{\lambda} \tag{29}$$

$$Relative\ Error = \frac{|Nu_{Pred} - Nu_{Exp}|}{Nu_{Exp}}\, 100\% \tag{30}$$

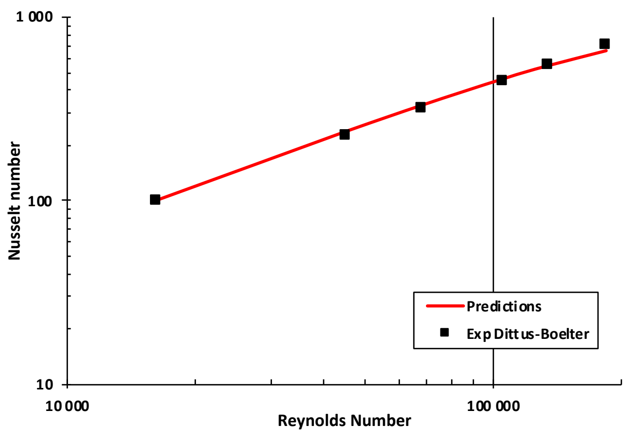

Figure 4. Validation of numerical predictions of the Nusselt number for carrier liquid flow. D = 0.026 m; T_w = 293.15 K, q = 1500 W/m.

It is seen in Figure 4 that the numerical computations of Nusselt number are close to the Dittus–Boelter data, and the averaged relative error, expressed by Equation (30), is about 2%.

3. Results of Predictions

Numerical predictions were performed based of the simplified mathematical model that contains Equations (10), (11), (16), (17), and the turbulence-damping Function (15). Predictions were made for four slurries. In each case, the slurry flow was fully developed hydrodynamically and thermally in a vertical upward pipeline with an inner diameter

D = 0.026 m. The wall temperature and the unit heat flux were constant and equal to 293.15 K and 1500 W/m, respectively. Simulations were performed for solid volume concentrations equal to 10%, 30%, and 40% by volume, and for water. The thermal properties of the solid and liquid phases and slurry were stated in Tables 1 and 2.

The results of the predictions of Nu = f(Re) for medium and coarse slurries at C = 10%, 30%, and 40% are presented in Figures 5 and 6. The Nusselt number for the carrier liquid (water) was calculated using the empirical Dittus–Boelter Equation (27).

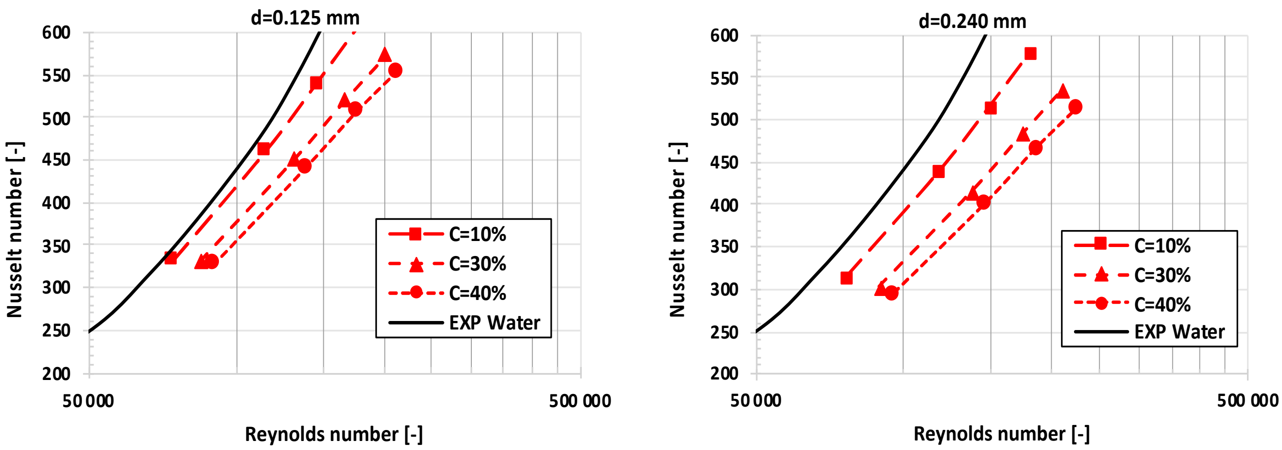

(**a**) (**b**)

Figure 5. Dependence of the Nusselt number on the Reynolds number for glass spheres slurries and water: (**a**) d = 0.125 mm and C = 10%, 30%, 40%; (**b**) d = 0.240 mm and C = 10%, 30%, 40%.

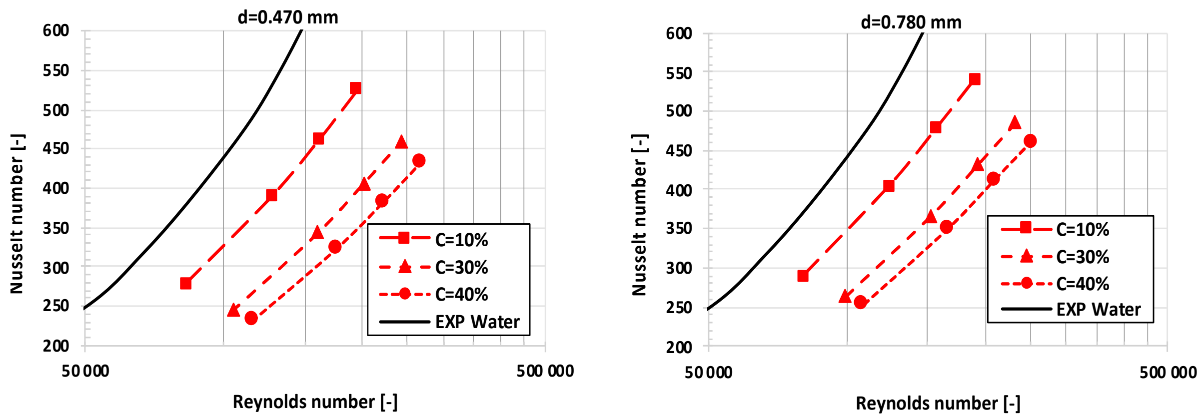

(**a**) (**b**)

Figure 6. Dependence of the Nusselt number on the Reynolds number for sand slurries and water: (**a**) d = 0.470 mm and C = 10%, 30%, 40%; (**b**) d = 0.780 mm and C = 10%, 30%, 40%.

Figures 5 and 6 demonstrate that parameters such as Re, d, and C strongly affect the Nusselt number. For all four slurries, the Nusselt number was lower compared to water. It is seen that with an increase in solid particle diameter from 0.125 mm to 0.470 mm, the Nusselt number decreases, while for d > 0.470 mm there is an increase.

The influence of particle diameter on the Nusselt number is clearly seen in Figure 7a,b. Both figures present predictions for the four slurries at C = 10% and C = 40%, respectively. Analysing Figures 2 and 3 and Figure 7a,b, it is seen that there is a correlation between frictional pressure loss and the Nusselt number. For example, for solid concentration C = 40%, it can be seen that the friction loss decreases if the diameter of the solid particles increases from d = 0.125 mm to d = 0.470 mm (Figures 2a and 3a) and increases if d > 0.470 mm (Figure 3b). The same applies to the Nusselt number, which is seen in Figure 7b.

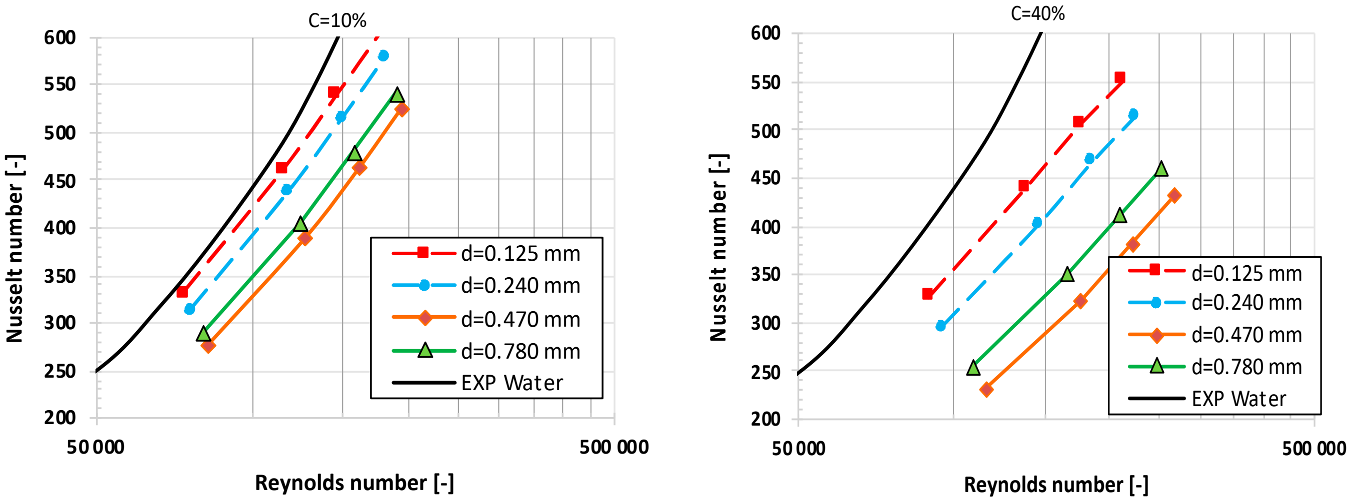

(**a**) (**b**)

Figure 7. Dependence of the Nusselt number on the Reynolds number for four slurries: (**a**) C = 10%; (**b**) C = 40%.

The relation of dp/dx = f(U_b) determines the link Nu = f(Re). Therefore, it is interesting to analyse the dependence of the Nusselt number on particle diameter for chosen solid concentrations and for chosen values of dp/dx, which is presented in Figure 8a,b and Figure 9a.

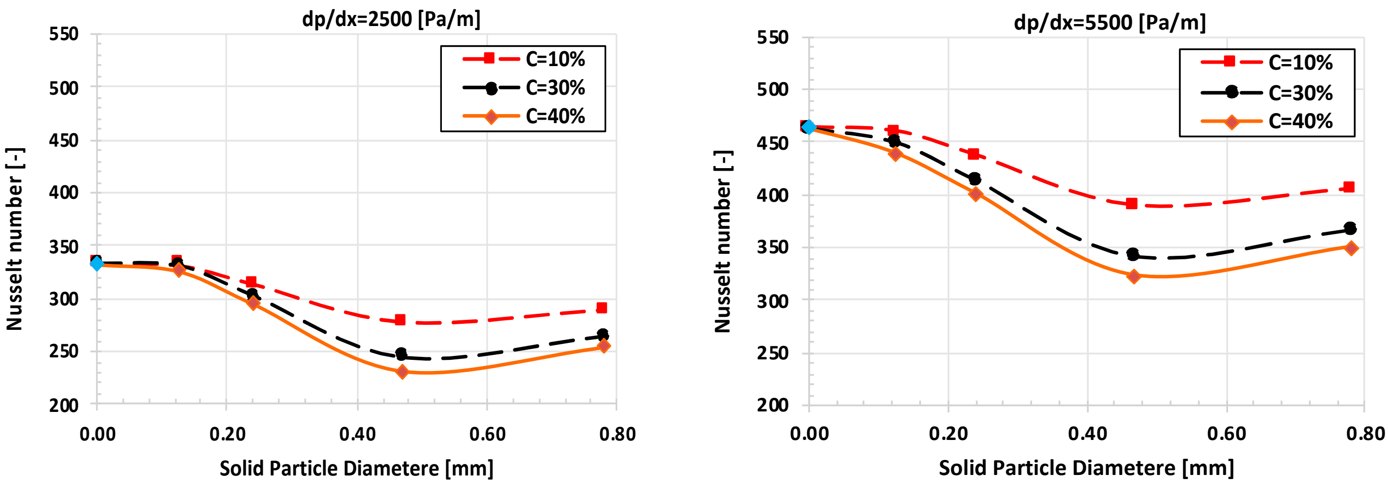

(**a**) (**b**)

Figure 8. Dependence of the Nusselt number on the particle diameter for four slurries and water: (**a**) dp/dx = 2500 Pa/m, C = 10%, 30%, 40%; (**b**) dp/dx = 5500 Pa/m, C = 10%, 30%, 40%.

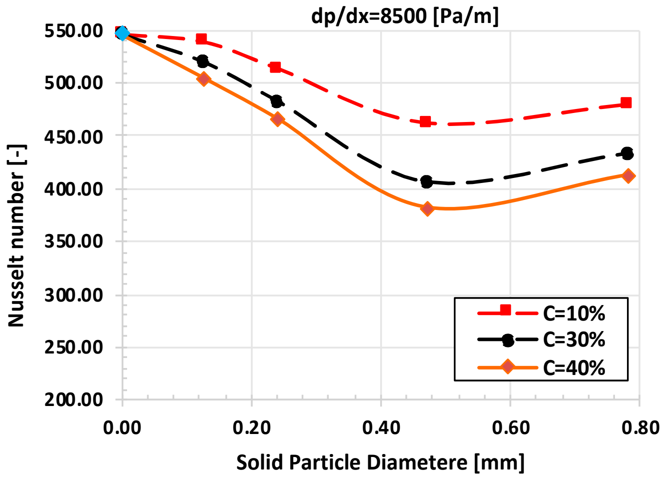

(**a**)

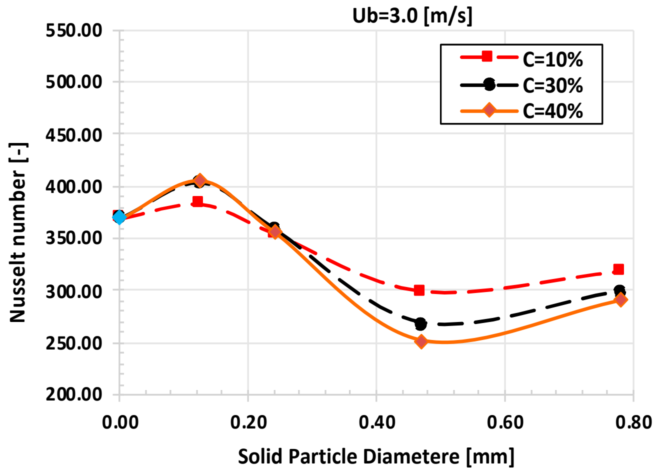

(**b**)

Figure 9. Dependence of the Nusselt number on the particle diameter for four slurries and water: (**a**) dp/dx = 8500 Pa/m, C = 10%, 30%, 40%; (**b**) U_b = const = 3.0 m/s and C = 10%, 30%, 40%.

Figure 8a,b and Figure 9a demonstrate that an increase in dp/dx causes an increase in the Nusselt number, while an increase in solid concentration causes a decrease in the Nusselt number. The first point in Figure 8a,b and Figure 9a, that is, for d = 0.0 mm, presents the data for the water, which were calculated using the Dittus–Boelter Equation (27). Analysis of Figure 8a,b and Figure 9a indicates that in the range of d = (0.125−0.780) mm, a minimum Nusselt number appears for d = 0.470 mm, regardless of solid concentration, while there is a maximum for water. This phenomenon is consistent with the behaviour of the pressure drop, which is presented in Figures 2 and 3.

It is interesting to analyse the behaviour of the Nusselt number for constant bulk velocity. Figure 9b presents the Nusselt number's dependence on the solid particle's diameter at constant bulk velocity equal to 3.0 m/s, and for C = 10%, 30%, and 40%, and for water. Again, the first point in Figure 9b shows the predictions for water (d = 0.0 mm). Figure 9b shows that with an increase in particle diameter from d = 0.0 mm (water) to d = 0.125 mm, the Nusselt number increases and reaches a maximum for d = 0.125 mm, regardless of solid concentration. If the particle diameter increases from d = 0.125 mm to d = 0.470 mm the Nusselt number decreases and reaches a minimum for d = 0.470 mm, irrespective of the solid concentration. Figure 9b shows that for constant bulk velocity (constant flow rate), the maximum and minimum of the Nusselt number exist for d = 0.125 mm and d = 0.470 mm, respectively. The maximum and minimum Nusselt numbers are consistent with the behaviour of the frictional pressure drop, which has been discussed earlier.

To illustrate why the efficiency of heat exchange between the pipe and the slurry is highest for d = 0.125 mm and the lowest for d = 0.470 mm, Figure 10 presents the temperature distributions for both slurries at C = 40% and U_b = 3.0 m/s. Taking into account Equation (18), it can be concluded that for constant heat flux, the coefficient of convective heat transfer is higher for the slurry with d = 0.125 mm compared to the slurry with d = 0.470 mm because $T_w - T_b$ is lower for the slurry with d = 0.125 mm than for d = 0.470 mm.

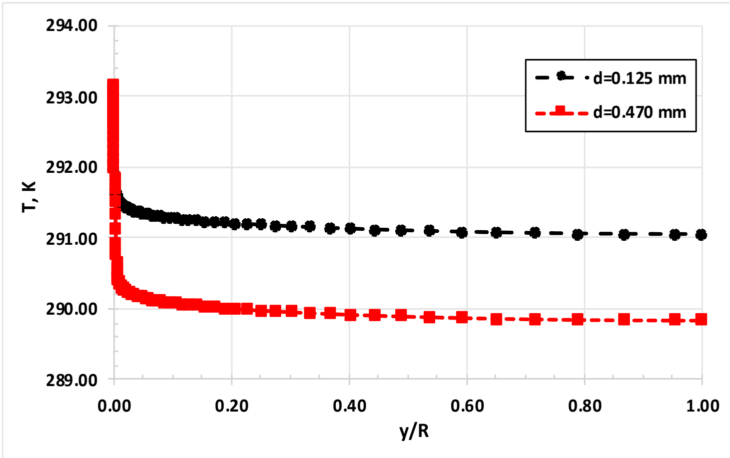

Figure 10. Temperature distributions for two slurries: with d = 0.125 mm; d = 0.470 mm; at U_b = 3.00 m/s, and C = 40%.

4. Discussion

It is well-known that fine solid particles can move freely in the viscous sublayer, and the friction process is similar to the flow of the carrier liquid. If sufficiently large particles, such as those used in this study, are considered, such particles are pushed away from the wall toward the symmetry axis, causing a decrease in the friction between the particles and the wall, and modifying the turbulence in the remaining region. Experiments have shown that, in some cases, the friction in the slurry can be lower than we expected. Such a phenomenon was observed in experiments of Charles and Charles [78] for d = 0.216 mm, Ghosh and Shook [79] for d = 0.6 mm, Matousek [36] for d = 0.37 mm, Sumner [40] for d = 0.47 mm, and d = 0.78 mm, Talmon [80] for d = (0.1–2.0) mm, and Ming-zhi et al. [81] for d = 0.125 mm and d = 0.44 mm. The process of enhancement or suppression of turbulence, caused by the presence of solid particles in the carrier liquid, is complex, especially in the viscous sublayer and buffer layer, and is still not well understood. For such complex phenomena, it is impossible to propose a universal approach to predict frictional loss or heat transfer.

This study showed that a mathematical model that uses a standard turbulence-damping function is not suitable for predicting the isothermal flow of a slurry with medium and coarse solid particles. Thus, it cannot be used to predict heat transfer. However, using the specially designed turbulence-damping function, described by Equation (15), allows one to apply a mathematical model to predict isothermal and non-isothermal slurry flow. However, it should be noted that the mathematical model assumes that the solid concentration across the pipeline is constant. In contrast, the experiments proved that the distribution is not constant, and the lowest concentration appears close to the pipe wall. The effect of non-uniform concentration distribution is compensated by the wall damping function, described by Equation (15).

Analysis of the literature indicates that the simplest way to formulate a mathematical model is to use the assumptions of constant heat flux acting on a unit of pipe length and constant wall temperature [47]. This approach was just used in this study. Looking for simplifications, the convective term in the energy equation was developed based on the heat balance between the pipe and the slurry. This approach allows one to reduce the mathematical model to one-dimensional and decrease the time of computation, causing the model to be convenient for parametric studies. The mathematical model allows for predicting the frictional pressure loss, profiles of velocity and temperature, and the Nusselt number. It is essential to emphasise that the mathematical model for heat exchange in a slurry flow should first be validated for the isothermal flow. The applied mathematical model is simple and suitable for predicting heat transfer in a medium or coarse slurry if the assumptions stated in the physical model are used. However, this model still requires validation for heat transfer if experimental data will be available. It is worth mentioning that the physical properties of slurries with glass spheres and sand particles are remarkably similar. Differences in the specific heat and thermal conductivity are minor, and the relative discrepancy is below 2.5%, while the discrepancy is about 8% for particles density.

Performed studies demonstrate that the median particle diameter of solid particles plays a substantial role in heat exchange in a slurry flow. The Nusselt number decreases in some cases; in the other cases, it increases with the change in the diameter of the solid particles. These anomalies indicate that the diameter of the solid particle affects frictional losses and is related to the physics of heat transfer and needs further study. The novelty and value of this study lies in the deeper characterisation of the influence of medium- and coarse-solid particles on heat exchange between pipe wall and slurry.

5. Conclusions

Analysis of the results of numerical predictions of heat exchange in turbulent flow of four slurries containing glass particles with d = 0.125 mm and d = 0.240 mm and sand particles with d = 0.470 mm and d = 0.780 mm in a vertical pipe directed upwards allows the following conclusions to be drawn:

- The diameter of the solid particle affects the Nusselt number and the friction loss, regardless of the concentration of the solids.
- The higher the solid concentration in the slurry, the lower the Nusselt number.
- In the chosen range of median particle diameters, the Nusselt number changed sinusoidal, reaching maximum for the slurry with d = 0.125 mm, and minimum for d = 0.470 mm.
- It was found that for the same volume of transported slurry (U_b = const), the efficiency of heat transfer is the highest for the slurry with *d* = 0.125 mm, while for the slurry with d = 0.470 mm *it* is the lowest—see Figures 9b and 10.
- The influence of the particle diameter on the Nusselt number and friction losses result in the impact of the particles on the turbulence. The suppression of turbulence was determined indirectly based on frictional loss analysis.
- Solid particles with a diameter of 0.470 mm demonstrate the highest suppression of turbulence and, consequently, suppression of heat transfer.

The results obtained can serve as a reference for further study of the resistance mechanism and the enhancement or suppression of heat transfer in the transported slurry through the presence of selected solid particles. Future research should focus on a deeper understanding of the mechanism of influence of particle size, density, and shape on turbulence, especially in the region close to a pipe wall. Research on the impact of physical and thermal properties of solid particles on the transport capability of solid particulates in different Prandtl liquids to minimise pressure loss and increase or decrease heat exchange is also needed.

Funding: The research was funded by Ministry of Education and Science, grant number 01.0.00.00/1.02.001/SUBB.M 23.002.

Data Availability Statement: Data are contained within this article.

Conflicts of Interest: The author declares no conflict of interest.

Nomenclature

A	cross section of the pipe, m^2
A_P	constant in the turbulence damping function (A_P = 100)
A_*	pipe surface over distance L = 1 m, m^2
a, b, c	constants in Taylor expansion

C_i	constant in Launder and Sharma turbulence model, i = 1, 2
C	solids concentration (volume fraction of solids averaged in cross-section), %
c_p	specific heat at constant pressure, J/(kg K)
D	inner pipe diameter, m
d	median solid particle diameter, mm
f_μ	turbulence damping function
g	specific gravity, m/s^2
j	nodal point
k	kinetic energy of turbulence, m^2/s^2
L	unit pipe length / length of mixing in Nikuradse formula, m
$\dot{m}$	flux of slurry mass, kg/s
n	number of iteration cycle
Nu	Nusselt number
Pr	Prandtl number
p	static pressure, Pa
q	input power of heat per unit pipe length (unit heat flux), W/m
R	pipe radius, m
r	cylindrical coordinate, distance from symmetry axis, m
Re	Reynolds number
t′	fluctuating component of temperature, K
T	temperature, K
$U_{i,j}$	time averaged velocity components, where U = f(U, V, W), m/s
U	velocity component in the main flow direction '0x', m/s
V	velocity component in the direction '0r', m/s
W	velocity component in the direction '0φ', rad/s
u′, v′	fluctuating components of velocity U, and V, respectively, m/s
x	cylindrical coordinate, main flow direction, m
y	radial distance from a pipe wall, m
$\overline{}$	time averaged
Greek symbols	
α	convective heat transfer coefficient, W/(m^2 K)
δ_{ij}	Kronecker quantity
Δx	unit pipe length, m
ε	rate of dissipation of kinetic energy of turbulence, m^2/s^3
λ	thermal conductivity of water or slurry, W/(m K)
μ	dynamic viscosity coefficient for water, Pa·s
ν	kinematic viscosity coefficient for water, m^2/s
ρ	density, kg/m^3
σ_i	diffusion coefficients in k-ε turbulence model, i = k, ε
τ	shear stress, Pa
Φ	general dependent variable, $\Phi = \rho, c_p, \lambda$
ϕ	general dependent variable, $\Phi = U, k, \varepsilon$
φ	cylindrical coordinate, angle around pipe symmetry axis, deg
Subscripts	
b	bulk (cross-section averaged value)
EXP	experiment
i	index, i = 1, 2
j	number of nodal points
L	liquid
m	slurry (solid–liquid mixture)
n	number of iterations
P	solid particle/solid phase
Pred	predictions
r	radius
t	turbulent
w	wall

References

1. Sape Miedema, P.A. *Slurry Transport: Fundamentals, Historical Overview and Delft Head Loss and Limit Deposit Velocity Framework*; TU Delft Open: Delft, The Netherlands, 2016; ISBN 9789461862938.
2. Zengeni, B.; Nekhavhambe, D.; Goosen, P. Sensitivity of non-Newtonian slurry viscous properties to temperature. In Proceedings of the 19th Conference on Transport and Sedimentation of Solid Particles, Cape Town, South Africa, 24–27 September 2019; pp. 285–292.
3. Dai, Y.; Zhang, Y.; Li, X. Numerical and experimental investigations on pipeline internal solid-liquid mixed fluid for deep ocean mining. *Ocean Eng.* **2021**, *220*, 108411. [CrossRef]
4. Wang, R.; Zhu, Z.; Su, X.; Mianowicz, K. Slurry pumps in deep-sea mining: A review of numerical and experimental studies. *Ocean Eng.* **2022**, *251*, 111150. [CrossRef]
5. Shook, C.A.; Roco, M.C. *Slurry Flow: Principles and Practice. Howard Brenner*; Digital Press: Clifton, NJ, USA, 2013; Available online: https://www.perlego.com/book/1884007/slurry-flow-principles-and-practice-pdf (accessed on 3 September 2023).
6. Baha, A.P.E. *Slurry Systems Handbook*, 2nd ed.; McGraw Hill: New York, NY, USA, 2021.
7. Reddy, N.V.K.; Pothal, J.K.; Barik, R.; Senapati, P.K. Pipeline slurry transportation system: An overview. *J. Pipeline Syst. Eng. Pract.* **2023**, *14*, 1–10. [CrossRef]
8. Csengeri, E. Fuel Discharge towards the Core Catcher in Sodium-Cooled Fast Reactor under Severe Accident Conditions with Mitigation Devices. Ph.D. Thesis, Université Grenoble Alpes, Grenoble, France, 2022.
9. Dong, H.; Aziz, N.A.; Shafri, H.Z.M.; Ahmad, K.A.B. Numerical study on transportation of cemented paste backfill slurry in bend pipe. *Processes* **2022**, *10*, 1454. [CrossRef]
10. Wilson, K.C.; Addie, G.R.; Sellgren, A.; Clift, R. *Slurry Transport Using Centrifugal Pumps*, 3rd ed.; Springer: Berlin/Heidelberg, Germany, 2006; Available online: https://link.springer.com/book/10.1007/b101079 (accessed on 3 September 2023).
11. Chen, Z.X.; Hu, H.X.; Guo, X.M.; Zheng, Y.G. Effect of groove depth on the slurry erosion of V-shaped grooved surfaces. *Wear* **2022**, *488–489*, 204133. [CrossRef]
12. Zhang, R.; Sun, L.; Li, Y.; Yin, J. Numerical analysis of solid particle erosion caused by slurry in dredging pipelines based on a particle separation method. *Powder Technol.* **2023**, *428*, 118826. [CrossRef]
13. Shaukat, R.; Qamar, A.; Anwar, Z.; Imran, S.; Amjad, M.; Ali, H.M. Experimental study on heat transfer performance of mPCM slurry flow in microchannels. *J. Therm. Anal. Calorim.* **2023**, 1–13. [CrossRef]
14. Rogachevskii, I. *Introduction to Turbulent Transport of Particles, Temperature and Magnetic Fields Analytical Methods for Physicists and Engineers*; Cambridge University Press: Cambridge, UK, 2021. [CrossRef]
15. Ahmed, J. *Rheology and Rheological Measurements*; Wiley: Hoboken, NJ, USA, 2021. [CrossRef]
16. Jorge, O. *Particle-Laden Turbulent Pipe Flows*; OmniScriptum GmbH Co.: Riga, Latvia, 2017.
17. Minier, J.P.; Pozorski, J. *Particles in Wall-Bounded Turbulent Flows: Deposition, Re-Suspension and Agglomeration*; Springer International Publishing: Cham, Switzerland, 2017; p. 261. [CrossRef]
18. Soo, S.L. *Instrumentation for Fluid Particle Flow*; University Press of Mississippi: Jackson, MS, USA, 2013.
19. Silva, R. Experimental characterization techniques for solid-liquid slurry flows in pipelines: A Review. *Processes* **2022**, *10*, 597. [CrossRef]
20. Mallach, M.; Gevers, M.; Gebhardt, P.; Musch, T. Fast and precise soft-field electromagnetic tomography systems for multiphase flow imaging. *Energies* **2018**, *11*, 1199. [CrossRef]
21. Ahmadi, F.; Ebrahimian, M.; Sanders, R.S.; Ghaemi, S. Particle image and tracking velocimetry of solid-liquid turbulence in a horizontal channel flow. *Int. J. Multiph. Flow* **2019**, *112*, 83–99. [CrossRef]
22. Hampel, U.; Barthel, F.; Bieberle, A.; Bieberle, M.; Boden, S.; Franz, R.; Neumann-Kipping, M.; Tas-Köhler, S. Tomographic Imaging of Two-Phase Flow. *Int. J. Adv. Nucl. React. Des. Technol.* **2020**, *2*, 86–92. [CrossRef]
23. Zou, J.; Liu, C.; Wang, H.; Wu, Z.P. Mass Flow Rate Measurement of bulk solids based on microwave tomography and microwave Doppler methods. *Powder Technol.* **2020**, *360*, 112–119. [CrossRef]
24. Yianneskis, M.; Whitelaw, J.H. Velocity characteristics of pipe and jet flows with high particle concentration. *ASME Symp. Liq. Solid Flows Eros. Wear Ind. Equip.* **1983**, *13*, 12–15.
25. Chen, R.C.; Kadambi, J.R. Discrimination between solid and liquid velocities in slurry flow using Doppler Velocimeter. *ASME Powder Technol.* **1995**, *85*, 127–134. [CrossRef]
26. Lv, Y.; Su, X.; Yang, H.; Zhang, J.; Wang, R.; Zhu, Z. Velocity slip in a deep-sea slurry pump and its effect on particle transportation. *J. Appl. Fluid Mech.* **2023**, *16*, 1654–1665. [CrossRef]
27. Nouri, J.M.; Whitelaw, J.H.; Yianneskis, M. Particle motion and turbulence in dens two-phase flows. *Int. J. Multiph. Flow* **1987**, *13*, 729–739. [CrossRef]
28. Schreck, S.; Kleis, S.J. Modification of grid-generated turbulence by solid particles. *J. Fluid Mech.* **1993**, *249*, 665–688. [CrossRef]
29. Chen, R.C.; Kadambi, J.R. Experimental and numerical studies of solid-liquid pipe flow. *ASME. Liq. Solid Flows* **1994**, *189*, 123–135. Available online: https://www.osti.gov/biblio/110079 (accessed on 3 September 2023).
30. Gai, G.; Hadjadj, A.; Kudriakov, S.; Thomine, O. Particles-induced turbulence: A critical review of physical concepts, numerical modeling and experimental investigations. *Theor. Appl. Mech. Lett.* **2020**, *10*, 241–248. [CrossRef]
31. Gore, R.A.; Crowe, C.T. Modulation of turbulence by a dispersed phase. *J. Fluid Eng.* **1991**, *113*, 304–307. [CrossRef]

32. Jianren, F.; Junmei, S.; Youqu, Z.; Kefa, C. The effect of particles on fluid turbulence in a turbulent boundary layer over a cylinder. *Acta Mech. Sin.* **1997**, *13*, 36–43. [CrossRef]
33. Eaton, J.K.; Paris, A.D.; Burton, T.M. Local distortion of turbulence by dispersed particles. *AIAA* **2012**, AIAA-99–3643. [CrossRef]
34. Fessler, J.R.; Eaton, J.K. Turbulence modification by particles in a backward-facing step flow. *J. Fluid Mech.* **1999**, *394*, 97–117. [CrossRef]
35. Li, D.; Luo, K.; Fan, J. Modulation of turbulence by dispersed solid particles in a spatially developing flat-plate boundary layer. *J. Fluid Mech.* **2016**, *802*, 359–394. [CrossRef]
36. Matousek, V. Research developments in pipeline transport of settling slurries. *Powder Technol.* **2005**, *156*, 43–51. [CrossRef]
37. Javed, K.; Vaezi, M.; Kurian, V.; Kumar, A. Frictional behaviour of wheat straw-water suspensions in vertical upward flows. *Biosyst. Eng.* **2021**, *212*, 30–45. [CrossRef]
38. Javed, K.; Kurian, V.; Kumar, A. The effect of particle size and concentration on the frictional behavior of vertical upward flows of wheat straw aqueous slurries. *Chem. Eng. Res. Des.* **2022**, *186*, 614–627. [CrossRef]
39. Nasr-El-Din, H.; Shook, C.A.; Colwell, J. The lateral variation of solids concentration in horizontal slurry pipeline flow. *Int. J. Multiph. Flow* **1987**, *13*, 661–670. [CrossRef]
40. Sumner, R.J. Concentration Variations and Their Effects in Flowing Slurries and Emulsions. Ph.D. Thesis, University of Saskatchewan, Saskatoon, SK, Canada, 1992.
41. Eaton, J.K.; Fessler, J.R. Preferential concentration of particles by turbulence. *Int. J. Multiph. Flow* **1994**, *20*, 169–209. [CrossRef]
42. Eskin, D.; Miller, M.J. A model of non-Newtonian slurry flow in a fracture. *Powder Technol.* **2008**, *182*, 313–322. [CrossRef]
43. Silva, R.; Garcia, F.A.P.; Faia, P.M.G.M.; Rasteiro, M.G. Settling suspensions flow modelling: A Review. *KONA Powder Part. J.* **2015**, *32*, 41–56. [CrossRef]
44. Cotas, C.; Asendrych, D.; Garcia, F.; Faia, P.; Rasteiro, M.G. COST Action FP1005. In Proceedings of the Final Conference EUROMECH Colloquium 566, Trondheim, Norway, 9–11 June 2015; pp. 31–33.
45. Chang, K.C.; Hsieh, W.D.; Chen, C.S. A modified low-Reynolds-number turbulence model applicable to recirculating flow in pipe expansion. *J. Fluids Eng.* **1995**, *117*, 417–423. [CrossRef]
46. Bartosik, A. Mathematical modelling of slurry flow with medium solid particles. In Proceedings of the 2nd International Conference on Mathematical Models for Engineering Science, Puerto de la Cruz, Spain, 10–12 December 2011; pp. 124–129.
47. Cieslinski, J. Numerical modelling of forced convection of nanofluids in smooth, round tubes: A review. *Energies* **2022**, *15*, 7586. [CrossRef]
48. Abidi, A.; Sajadi, S.M. Impact of fin and hybrid nanofluid on hydraulic-thermal performance and entropy generation in a solar collector using a two-phase approach. *Eng. Anal. Bound. Elem.* **2023**, *156*, 311–320. [CrossRef]
49. Bordet, A.; Poncet, S.; Poirier, M.; Galanis, N. Advanced numerical modeling of turbulent ice slurry flows in a straight pipe. *Int. J. Therm. Sci.* **2018**, *127*, 294–311. [CrossRef]
50. Hassaan, A.M. Comparing the performance of using nanofluids in two different types of heat exchangers with the same heat transfer area. *Heat Transf. Res.* **2023**, *54*, 1–16. [CrossRef]
51. Mandal, D.K.; Hazra, A.; Biswas, N. Effect of particle size on fluid flow and heat transfer in a pipe with slurry flow. *IOP Conf. Ser. Mater. Sci. Eng.* **2021**, *1080*, 012026. [CrossRef]
52. Harada, E.; Toda, M.; Kuriyama, M.; Konno, H. Heat transfer between wall and solid-water suspension flow in horizontal pipes. *J. Chem. Eng.* **1985**, *18*, 33–38. [CrossRef]
53. Iqbal, M.; Kouloulias, K.; Sergis, A.; Hardalupas, Y. Critical analysis of thermal conductivity enhancement of alumina–water nanofluids. *J. Therm. Anal. Calorim.* **2023**, *148*, 9361–9389. Available online: https://link.springer.com/article/10.1007/s10973-023-12334-7 (accessed on 14 July 2023). [CrossRef]
54. Hetsroni, G.; Rozenblit, R. Heat transfer to a solid-liquid mixture in a flume. *Int. J. Multiph. Flow* **1994**, *20*, 671–689. [CrossRef]
55. Rozenblit, R.; Simkhis, M.; Hetsroni, G.; Taitel, Y. Heat transfer in horizontal solid-liquid pipe flow. *Int. J. Multiph. Flow* **2000**, *26*, 1235–1246. [CrossRef]
56. Bhanvase, B.; Barai, D. *Nano Fluid for Heat and Mass Transfer—Fundamentals. Sustainable Manufacturing and Applications*; Academic Press in an imprint Elsevier: London, UK, 2021; p. 448. Available online: https://www.elsevier.com/books-and-journals (accessed on 30 April 2021).
57. Permanasari, A.A.; Faridi, A.F.; Sukarni, S.; Puspitasari, P.; Mohamed, N.M.; Pratama, M.M.A. Heat transfer characteristics on shell and tube heat exchanger using TiO2/water-ethylene glycol nanofluid. *AIP Conf. Proc.* **2023**, *2748*, 020048. [CrossRef]
58. Firdaus, D.R.; Permanasari, A.A.; Sukarni, S.; Puspitasari, P. Heat transfer performance of DWCNTs nanofluids in shell and tube heat exchanger with segmental baffle. *AIP Conf. Proc.* **2023**, *2687*, 040023. [CrossRef]
59. Sattar, E.A.; Ouda, A.A.; Salman, M.D. Enhancement heat transfer in shell and tube heat exchanger by used hybrid and nanofluid. *AIP Conf. Proc.* **2023**, *2787*, 030006. [CrossRef]
60. Wang, X.; Xu, X.; Choi, S.U.S. Thermal conductivity of nanoparticle—fluid mixture. *J. Thermophys. Heat Transfer.* **1999**, *13*, 474–480. [CrossRef]
61. Lotfi, R.; Saboohi, Y.; Rashidi, A.M. Numerical study of forced convective heat transfer of nanofluids: Comparison of different approaches. *Int. Commun. Heat Mass Transf.* **2010**, *37*, 74–78. [CrossRef]
62. Mokmeli, A.; Saffar-Avval, M. Prediction of nanofluid convective heat transfer using the dispersion model. *Int. J. Therm. Sci.* **2010**, *49*, 471–478. [CrossRef]

63. Shook, C.A.; Bartosik, A.S. The pseudohomogeneous flow approximation for dispersed two-phase systems. *Part. Sci. Tech.* **1991**, *9*, 119–134. [CrossRef]
64. Boussinesque, J. Theorie de l'ecoulement tiurbillant. *Mem. Acad. Sci.* **1877**, *23*, 46.
65. Blom, J. Experimental determination of the turbulent Prandtl number in a developing temperature boundary layer. In Proceedings of the 4th International Conference Heat Transfer, Paris, France, 31 August–5 September 1970; Volume VII.
66. Launder, B.E.; Sharma, B.I. Application of the energy-dissipation model of turbulence to the calculation of flow near a spinning disc. *Lett. Heat Mass Transfer.* **1974**, *1*, 131–138. Available online: https://www.sciencedirect.com/science/article/abs/pii/0094454874901507 (accessed on 7 August 2021). [CrossRef]
67. Mathur, S.; He, S. Performance and implementation of the Launder–Sharma low-Reynolds number turbulence model. *Comput. Fluids* **2013**, *79*, 134–139. [CrossRef]
68. Lawn, C.J. The determination of the rate of dissipation in turbulent pipe flow. *J. Fluid. Mech.* **1971**, *48*, 477–505. [CrossRef]
69. Cotas, C.; Asendrych, D.; Garcia, F.A.P.; Fala, P.; Rasteiro, M.G. Turbulent flow of concentrated pulp suspensions in a pipe—Numerical study based on a pseudo-homogeneous approach. In Proceedings of the COST Action FP1005 Final Conference, EUROMECH Colloquium 566, Trondheim, Norway, 9–11 June 2015; Available online: https://www.researchgate.net/publication/283342328 (accessed on 7 August 2021).
70. Cotas, C.; Silva, R.; Garcia, F.; Faia, P.; Asendrych, D.; Rasteiro, M.G. Application of different low-Reynolds k-ε turbulence models to model the flow of concentrated pulp suspensions in pipes. *Procedia Eng.* **2015**, *102*, 1326–1335. [CrossRef]
71. Abir, I.A.; Emin, A.M. A comparative study of four low-Reynolds-number k-e turbulence models for periodic fully developedduct flow and heat transfer. *Numer. Heat Transf. Part B Fundam.* **2016**, *69*, 234–248.
72. Bartosik, A. Validation of friction factor predictions in vertical slurry flows with coarse particles. *J. Hydrol. Hydromech.* **2020**, *68*, 119–127. [CrossRef]
73. Jones, T. Advances in Slurry Technology. In *Chapter: Numerical Modelling of Medium Slurry Flow in a Vertical Pipeline*; IntechOpen: London, UK, 2023; pp. 1–19. [CrossRef]
74. Roache, P.J. *Computational Fluid Dynamics*; Hermosa Publishing: Albuquerque, NM, USA, 1982.
75. Nikuradse, J. Unyersuchungen über die geshwindigkeitsverteilung in turbulenten strömungen. *Aeronaut. J.* **1927**, *31*, 1170. [CrossRef]
76. Hermandes-Peres, V.; Abdulkadir, M.; Azzopardi, B.J. Grid generation issues in the CFD modelling of two-phase flow in a pipe. *J. Comput. Multiph. Flows.* **2011**, *3*, 1–26. [CrossRef]
77. Dittus, F.W.; Boelter, L.M.K. Heat transfer in automobile radiators of the tubular type. *Int. Comm. Heat Mass Transfer.* **1985**, *12*, 3–22. [CrossRef]
78. Charles, M.E.; Charles, R.A. *Advances in Solid-Liquid Flow and Its Applications*; Pergamon Press: New York, NY, USA, 1971; Available online: https://www.elsevier.com/books/advances-in-solid-liquid-flow-in-pipes-and-its-application/zandi/978-0-08-015767-2 (accessed on 3 September 2023).
79. Ghosh, T.; Shook, C.A. Freight pipelines. In *Freight Pipelines*; Liu, H., Round, G.F., Eds.; Hemisphere: Washington, DC, USA, 1990; pp. 281–288.
80. Talmon, A.M. Analytical model for pipe wall friction of pseudo-homogenous sand slurries. *Part. Sci. Tech.* **2013**, *31*, 264–270. [CrossRef]
81. Li, M.-Z.; He, Y.-P.; Liu, W.-H.; Liu, Y.-D.; Huang, C.; Jiang, R.-H. Effect of adding finer particles on the transport characteristics of coarse-particle slurries in pipelines. *Ocean Eng.* **2018**, *2020*, 108160. [CrossRef]